JOURNAL OF MATERIALS SCIENCE 29 (1994) 754–761

A computer simulation method for sintering in three-dimensional powder compacts

W. J. SOPPE, G. J. M. JANSSEN, B. C. BONEKAMP, L. A. CORREIA, H. J. VERINGA
Netherlands Energy Research Foundation ECN, PO Box 1, 1755 ZG Petten, The Netherlands

A new simulation method for sintering in three-dimensional powder packings is presented. The model is based on two-particle sintering interactions and is able to describe mass transport mechanisms based on grain-boundary diffusion as well as on lattice diffusion. It is shown that the simulation method provides an adequate description of structural reorganization effects which occur during the early stage of sintering. Simulation results are presented for the sintering of a random packing and of some crystalline-type packings in which various initial defects have been created.

1. Introduction

The modelling of sintering processes has a history that goes back more than 45 years [1]. One of the main challenges through these years, has been to predict the structural reorganization effects, which occur during the sintering of irregular packings [2–5]. These reorganization effects lead to large fluctuations in the amount of shrinkage, and therefore have an enormous influence on the strength of the sintered material. Reorganization takes place when angles between connecting lines of particle centres change. The change in angle is typically a many-particle result: the process at one junction influences the net results at another. Note that for this to happen, different necks themselves need not overlap. Sintering models developed by other authors [6–8] have in common that the particle packing is treated essentially as an entity in the analysis of the sintering kinetics. Such a treatment either rules out the description of the effects of local inhomogeneities [6] or raises problems of topological character [7, 8].

The aim of the present work was the modelling of structural reorganization effects taking place in the early stage of sintering. A many-particle simulation model is presented, in which the sintering kinetics are described by a summation of local two-sphere interactions. This approach ensures that the simulation scheme, in principle, can be applied to any initial packing and that topological constraints intrinsically are obeyed.

The two-sphere interaction model is a description of the local mechanism of sintering at one grain-boundary area. In the past, many models for the two-sphere interaction have been proposed. In general, these models are based on thermodynamic and atomistic considerations, combining concepts of the driving force, i.e. minimization of the free energy of the surface, with material transport mechanisms. Well-known are the interaction models suggested by Coble [9] and Kingery and Berg [10] involving mass transport through grain-boundary diffusion, lattice diffusion and surface diffusion. Models based on material transport through viscous flow and through evaporation and recondensation have also been developed. A survey of these models can be found in the review paper by Exner [11]. In the present simulation scheme, any of these models can be implemented; the only restriction being that the neck formation is coupled to centre-to-centre approach.

The simulation scheme and its implementation is described first. Next, the simulations of sintering of a random packing and of some typical crystalline packings with various initial defects are presented and discussed.

2. Method

Consider a system of N equal spheres, each with radius R. The position of the ith particle at time t is denoted by $\boldsymbol{r}_i(t)$. As a result of local interactions with adjoining spheres, the coordinates of a sphere will change in time. The net displacement of a sphere i is given by

$$\frac{\mathrm{d}\boldsymbol{r}_i(t)}{\mathrm{d}t} = \sum_{i \neq j} f(r_{ij})\hat{\boldsymbol{r}}_{ij} \tag{1}$$

Here, $\boldsymbol{r}_{ij} = \boldsymbol{r}_i - \boldsymbol{r}_j$, $\hat{\boldsymbol{r}}_{ij}$ is the unit vector in the direction of $\boldsymbol{r}_{ij}$. The summation is restricted to particles j in contact with particle i, i.e. $f(r_{ij}) = 0$ for $r_{ij} > 2R$. The function $f(r_{ij})$ represents the local two-particle sintering interaction and will be discussed below. An iterative numerical integration scheme with discrete time steps Δt is employed to describe the configurational change during the sintering process. The time dependency of $\boldsymbol{r}_i(t)$ is approximated by the Taylor expansion

$$\boldsymbol{r}_i(t + \Delta t) = \boldsymbol{r}_i(t) + \mathrm{v}_i(t)\Delta t + \frac{1}{2}a_i(t)(\Delta t)^2 + \mathrm{O}(\Delta t)^3 \tag{2}$$

0022–2461

Using the Adams–Bashforth two-step method for integration [12], i.e. setting

$$a_i(t) = [v_i(t) - v_i(t - \Delta t)]/\Delta t \tag{3}$$

and substituting Equation 1 into Equation 2, one obtains

$$r_i(t + \Delta t) = r_i(t) + \Delta t \sum_{i \neq j} \left\{ \frac{3}{2} f[r_{ij}(t)] - \frac{1}{2} f[r_{ij}(t - \Delta t)] \right\} \hat{r}_{ij} \tag{4}$$

We now turn to the local two-sphere interaction model in which the mechanisms of the sintering are incorported. In Fig. 1 a section along a line between the centres of two spheres is shown. In general, the neck growth can be written as a rather simple function of time

$$\left(\frac{\rho}{R}\right)^n = \frac{C_M}{R^m} t \tag{5}$$

where m and n are exponents. The constant C_M contains physical quantities as surface tension, diffusivity and temperature. With the approximation $h = \rho^2/4R$ this can be rewritten as

$$\left(\frac{h}{R}\right)^{n/2} = \frac{C_M}{2^n R^m} t \tag{6}$$

where ρ is the neck radius, h is the interpenetration distance and t is the sintering time, cf. Fig. 1. In his review paper, Exner [11] has shown that the approximation $h = \rho^2/4R$ is applicable to situations far beyond the limit of $\rho/R < 0.3$. Hence, for the initial and intermediate stages of sintering, the approximation is valid.

It is now an easy matter to derive an expression for the local functions $f(r_{ij})$. For two interpenetrating spheres we can write

$$r_{ij} = 2R - 2h_{ij} \tag{7}$$

and hence

$$\frac{dr_{ij}}{dt} = -2\frac{dh_{ij}}{dt} \tag{8}$$

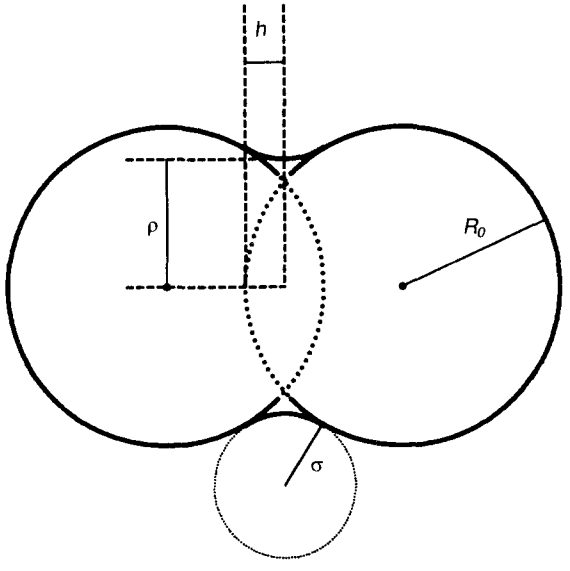

Figure 1 The two-body sintering model.

We have added the subscript ij to h in order to emphasize the fact that we are dealing with a pair property. From Equation 6 we find

$$\frac{dh_{ij}}{dt} = \frac{C_M}{n2^{n-1}R^{(2m-n)/2}} h_{ij}^{1-n/2} \tag{9}$$

or

$$\frac{dr_{ij}}{dt} = -\frac{C_M}{n2^{n-2}R^{(2m-n)/2}} h_{ij}^{1-n/2} \tag{10}$$

With $dr_{ij}/dt = 2f(r_{ij})$, we now can express $f[r_{ij}(t)]$ in terms of h_{ij}

$$f[r_{ij}(t)] = -\frac{C_M}{n2^{n-1}R^{(2m-n)/2}} h_{ij}^{1-n/2}(t). \tag{11}$$

With this result, the description of the simulation scheme is complete. Summarizing: at each given time t the value $h_{ij}(t)$ is calculated from each pair of touching spheres. Equations 4 and 11 then are used to update the coordinates and the whole procedure is repeated for time $t + \Delta t$.

The mechanism of vacancy diffusion from the neck zone determines the expression used for C_M, and the values for the exponents m and n. C_M, n and m can be derived from theoretical considerations, but very often they are obtained from experiments. Ranges for these exponents, as well as plausible values for C_M are given in the review by Exner [11]. In general, several diffusion mechanisms will occur at the same time and a linear combination of interaction models may be used. Models discussed by Exner include grain-boundary diffusion and lattice diffusion. For grain-boundary diffusion, with physical constant C_G, the values of the exponents are $m = 4$ and $n = 6$, leading to

$$f[r_{ij}(t)] = -\frac{C_G}{3 \cdot 2^6 R} h_{ij}^{-2}(t) \tag{12}$$

For lattice diffusion, with physical constant C_L, the values are $m = 3$ and $n = 4$, and hence

$$f[r_{ij}(t)] = -\frac{C_L}{32R} h_{ij}^{-1}(t). \tag{13}$$

Both these models are implemented in the present sintering program. The extension to other interaction models is straightforward.

To start the calculation, $f[r_{ij}(-\Delta t)]$ is assumed to be zero. A singularity exists when h_{ij} is zero as may easily occur at the start of the simulation. Therefore, in all calculations we replace h_{ij} by $(h_{ij} + \varepsilon R)$ where ε is an arbitrarily small number. The simulation ends either when a given maximum number of time steps has been achieved or when at some instance, locally, for one pair ij, a limiting value of h_{ij}/R is exceeded. The resulting configuration then can be analysed by calculating various characterizing quantities. In order to monitor configurational changes, several structural characteristics such as the overall shrinkage, the co-ordination number, G_i, and the densification, z_i, of every particle, are evaluated every n_m time steps. In this paper, the external sizes of the packing, determined by the extremes of the coordinates of the par-

ticles, are used for the evaluation of the shrinkage of the packing during the sintering. The densification parameter, z_i, of particle i, is defined as [13]

$$z_i = \frac{2R}{G_i} \sum_{j=1}^{G_i} \frac{1}{|r_{ij}|} \tag{14}$$

where the coordination number G_i is the number of neighbours j, with $|r_{ij}| \leq 2R$. The local density, ρ_i, associated with particle i then is $\rho_i = \rho_0 z_i^3$ where ρ_0 is the initial bulk density. The above mentioned limiting value of h_{ij}/R corresponds to $z_{\lim}$. By definition

$$z_{\lim} = \frac{R}{R - h_{ij}^{\lim}} \tag{15}$$

In practice, this parameter will be used in the simulations in order to determine where a run should be stopped.

3. Details of the simulations

The simulations are started by building a three-dimensional configuration consisting of a close packing of several hundreds of spherical particles. In this paper, we present simulations of regular, crystalline packings in which defects in the form of interfaces and vacancies are introduced, and a simulation of a random packing. At this initial stage, each particle is touching ($|r_{ij}| = 2R$) one or more neighbours. Now (at time $t = 0$), for each particle i, a list is made in which all neighbouring particles j with $|r_{ij}| \leq R_N$ are stored. In this paper, we have used $R_N = 2\sqrt{2}R$. In order to reduce computational efforts, we do not update these lists but we assume that during the entire simulation, only the particles contained in its initial neighbour list can interact (i.e. can come in contact) with a certain particle.

Then we start the simulation of the sintering kinetics. The net displacement of each particle i is calculated for many iteration steps, using Equation 4. The simulation examples in this paper are restricted to sintering processes controlled by grain-boundary diffusion; i.e. using Equation 12 as an expression for $f(r_{ij})$. An experimentally obtained value for alumina, has been substituted for C_G. As mentioned, we only have to evaluate h_{ij} for particles j which are in the initial neighbour list of particle i, which implies that the consumption of computer time increases linearly with N, the total number of particles.

The required computer time can be reduced further if one realizes that the sintering velocity is known to decrease exponentially. This velocity decrease justifies a likewise increase of the time step, Δt, after each iteration, n, i.e. $\Delta t_{n+1} = \Delta t_0 \cdot 10^{(an)}$. Δt_0 has to be chosen sufficiently small in order to obtain a reliable simulation of the crucial first stage of the sintering process. The value of a has been chosen such that $\Delta t_n = 1$ s for $n = 5000$ (see Table I). However, it may occur that during the sintering process, new contacts are created. In order to prevent unrealistic large displacements on both sides of this new grain boundary, the time step (for all particles) is set back to Δt_0 after such an event. After sufficiently many time steps (typically of the order 10^4) the simulation is terminated. A run of 20 000 time steps and 450 particles, required about 10 min CPU time on a Convex C-230 computer.

The crystalline model systems, we have simulated in this study, can be characterized as follows. Basic entities are (almost square) sections of the {0 0 1} planes in a f c c crystal, each consisting of 45 particles and with an external dimension of $9\sqrt{2}R \times 8\sqrt{2}R$ (see Fig. 2). If A refers to the (0 0 1) plane and B to the (0 0 2) plane, then a stacking sequence of ABABAB... (and a distance between the planes equal to $\sqrt{2}R$ gives rise to a face centred cubic (f c c) structure; AAAAA.... (and with plane distance $2R$) yields a simple cubic (s c) structure and ....ABABABAAAAAA.... describes a f c c–s c interface. In these structures, additional defects are created by removing from the central layer of a row of particles in either the ⟨1 0 0⟩, ⟨0 1 0⟩ or the ⟨1 1 0⟩ direction.

The random packing that has been simulated, was generated by using a deposition model and a consecutive compression model, described in a previous paper [14]. In the packings generated by these models, the particles do not touch their neighbours exactly; therefore, we have used for packing number 8 a value for ε that is slightly larger than for the simulations of the crystalline packings. Because the random packing is build up within a finite container, wall effects cause the mean volume fraction of this structure before

TABLE I Numerical values for parameters used in this work

C_G/R^4	4.1×10^{-5} s^{-1} [a]
ε	1.0×10^{-3} for the crystalline-type packings
	5.0×10^{-3} for the random packing.
Δt_0	$1.0 \times 10^{-13} R^4/C_G$ s
R_N	$2\sqrt{2}R$
a	$2{\cdot}10^{-4} \log(1/\Delta t_0)$ (resulting in $\Delta t_n = 1$ s for $n = 5000$)
n_m	4000
$z_{\lim}$	1.15

[a] Experimentally determined, non-isothermal bulk shrinkage for alumina ($T = 1500°$C); the corresponding mean particle size, R, measured with a Malvern Mastersizer, was 0.6 μm.

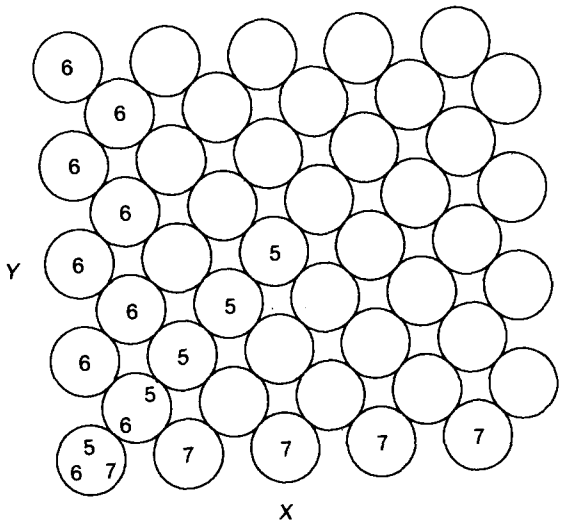

Figure 2 Basic layer A. The numbers refer to the structures in which the corresponding particles have been removed from the central layer.

TABLE II Characteristics of the model structures used in this work

Structure	Stacking sequence {0 0 1} planes	Defects[a]	Number of particles	External size (R^3) $X \times Y \times Z$	G_{mean}	Mean volume fraction[b]
1	AAAAAAAAAA	None	450	14.728 × 13.314 × 20.000	5.0000	0.4806
2	ABABABABAB	None	450	14.728 × 13.314 × 14.728	9.6400	0.6527
3	AAAAABABAB	I	450	14.727 × 13.314 × 17.657	7.0622	0.5444
4	ABABAAAAAABABAB	I	675	14.728 × 13.314 × 25.314	7.8163	0.5696
5	ABABAAAAAABABAB	I + 5[110]	670	14.728 × 13.314 × 25.314	7.8060	0.5654
6	ABABAAAAAABABAB	I + 9[010]	666	14.728 × 13.314 × 25.314	7.8198	0.5620
7	ABABAAAAAABABAB	I + 5[100]	670	14.728 × 13.314 × 25.314	7.8179	0.5654
8	Random packing		1000	17.000 × 17.000 × 29.796	3.4120	0.4864

[a] The defects refer to an interface (I) or to a missing row of particles in the layer that is central in the Z direction. 5[1 1 0] implies that in that layer, starting from $(X, Y) = (0, 0)$, a row of five particles in the [1 1 0] direction are missing. (See also Fig. 2.)
[b] The mean volume fraction is determined by the external dimensions of the simulation box. Owing to finite size effects, these values are smaller than for bulk materials. (For s c structures *cf.* 1, the bulk value is 0.524 and for f c c structures *cf.* 2, the bulk value is 0.740.)

sintering to be rather modest: 0.49. The value of the mean volume fraction is further reduced by the circumstance that the method of compression is less efficient at the top of the packing than at the bottom. In the lower regions of the packing, densities up to 0.60 can be observed.

In Table II, the pre-sintering characteristics of the model structures that we have simulated, are briefly presented. It should be noted that the external sizes of the packings, presented in this table, are upper limits determined by the extremes of the X, Y and Z coordinates of the particles and taking into account the radii of the particles. Consequently the volume fractions given can be considered as lower limits of the bulk values.

4. Results and discussion

The sintering simulation of each packing, described in Table II, has been continued until somewhere in the structure the limiting value of z ($z_{lim} = 1.15$) has been achieved. The crystalline type structures typically need a few thousand time steps to reach z_{lim}. During these sintering processes, no new particle contacts are created. The random packing, however, shows a rather different behaviour. Right from the beginning of the sintering, new particle contacts are created. Because Δt is set back to its initial value, Δt_0, each time a new particle contact arises, a larger number of time steps is required to simulate the same real sintering time as for the crystalline type packings. In fact, the simulation of the random packing required an amount of 370000 time steps.

The other sintering characteristics also show a quite different behaviour for the crystalline type structures than for the random packing. These differences are due to the fact that the crystalline type packings consist of one large cluster of connecting particles, where the random packing, due to its formation history, consists of many clusters of various size. Consequently, a displacement of a particle in a crystalline type packing will affect the position of all other particles of that packing, but in the random packing, the effect of a displacement of a particle is very local: it is restricted to the other particles of the same cluster.

In Table III, two typical sintering characteristics are presented: the real sintering time of the simulations and the volume shrinkage. In order to compare the sintering times of the packings, one should keep in mind that these sintering times, in fact, are determined by the fastest contracting pairs in the packing. The net displacement of a particle (see Equation 1) will be large if the position of its neighbours has a low mirror symmetry with respect to any plane through the particle itself. In regular crystalline packings, such particles are found near the surface but in the non-regular packings (3–7) such particles are also found in the vicinity of the interfaces or near vacancy defects. In the random packing, it is very probable that the pairs with the fastest contraction are present: isolated clusters consisting of two particles. These pairs are responsible for the very short sintering time of this structure. Later in this paper, we will provide some evidence for the existence of these small clusters. For the s c packing, a particle at the surface experiences only a net inward interaction from one particle, where for the f c c packing this number is 4. This explains the difference in the sintering times of structures 1 and 2. The introduction of an interface (structures 3 and 4) creates particles with even more net inward interacting neighbours; these particles can be found at the surface of the f c c sides of the interface. These interfaces, therefore, further decrease the sintering time. As the vacancy defects, introduced in structures 5–7, are present in the

TABLE III Volume shrinkage and sintering times of the model structures

Structure	Length shrinkage[a] (%)			Sintering time(s)
	X	Y	Z	
1	94.2	94.0	94.5	28.1
2	81.7	80.2	81.7	16.4
3	84.2	83.5	84.3	11.5
4	84.3	83.7	88.1	11.5
5	87.1	86.3	90.3	11.5
6	86.0	85.9	90.1	11.5
7	88.4	87.1	91.5	9.6
8	99.9	99.9	99.9	3.0

[a] The largest dimensions are taken into account.

s c layers, they do not contribute very much to the displacement of the particles with the largest inward motion because these particles still can be found in the f c c layers. This is reflected in net sintering times which are almost the same as for structures 3 and 4.

As mentioned above, the short sintering time for the random packing is most probably due to the presence of small, isolated clusters in this structure. These isolated clusters, which will also be present near the surface of the packing, are also responsible for the small shrinkage of the total volume as we have defined it. Because of their isolation, the net inward displacement of these clusters will be very small, keeping the outer volume of the whole packing almost unchanged. The behaviour of the volume shrinkage of the regular crystalline packings (1 and 2) is in accordance with their mean coordination number. The volume shrinkage of packing 3 is a mixture of the shrinkage of 1 and 2, where it should be taken into account that the shrinkage in the s c layer of the packing is enhanced by the presence of the f c c layer, which in its turn has a somewhat lower shrinkage than a regular f c c packing. For packing 4, a similar reasoning can be made, except for the shrinkage in the Z direction. Here, it can be noticed that the presence of two f c c layers, one at the top of and one below the s c layer, results in a nearly zero contraction of the s c layer in the Z direction. Finally, the volume shrinkage of packings 5, 6 and 7 show that the introduction of defects in the form of vacancies, locally may enhance the shrinkage but has a detrimental effect on the shrinkage of the outer volume.

Another interesting parameter of the sintering process is z_{mean}. In Fig. 3 this parameter is plotted as a function of the sintering time for all simulated structures. z_{mean}, better than the volume shrinkage as we have defined it, indicates the contraction of the *net* volume occupied by a packing. It can be observed that the minimum real volume shrinkage is obtained for the s c packing (1) where the f c c structure (2) yields the maximum real volume shrinkage. The net volume shrinkage of the other packings, including the random packing, is somewhere between these two extremes. Taking the s c packing (1) as a reference, we see that the random packing has a higher z_{mean} where its volume shrinkage is samller. This indicates that in the random packing, the pores have grown bigger. This is also the case for packings 5, 6 and 7, for which the volume shrinkage is smaller than for the vacancy-free packings 3 and 4, but which have a z_{mean} that is slightly larger.

As mentioned already, the mean coordination number of the random packing increases directly from the beginning of the simulation. In Fig. 4, G_{mean} is plotted versus the sintering time. It can be observed that G_{mean}, after a fast initial increase, grows rather slowly and even seems to go into saturation for sintering times beyond the present simulation time. Anyway, it is rather unlikely that the mean coordination number for this random packing will ever exceed a value of 4.0. This indicates that this random packing, after sintering, consists of many isolated clusters of particles. In Fig. 5, the distribution of the particles in the random

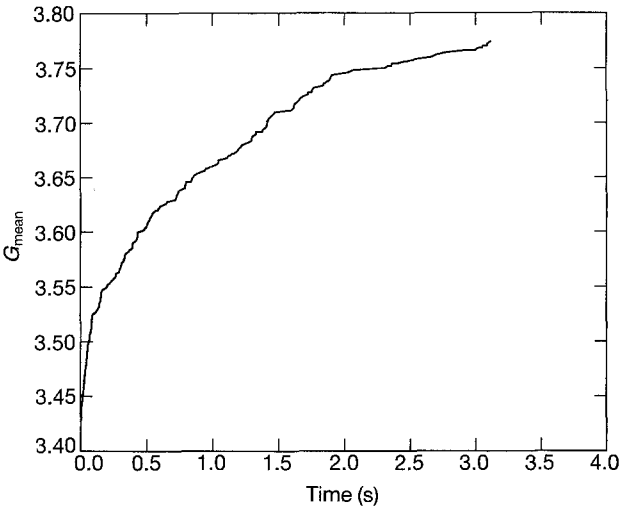

Figure 4 Mean coordination number of the random packing (8) versus sintering time.

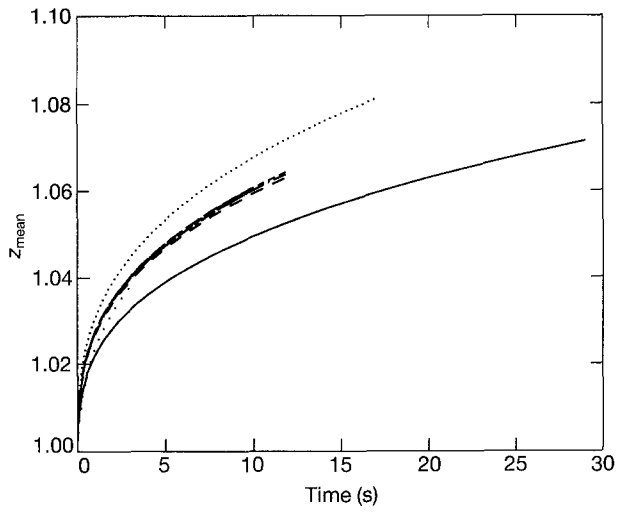

Figure 3 Mean value of local density, z, versus sintering time. (———) 1, (. . .) 2, (– – –) 3, (— — —) 4, (—•—) 5, (— — —) 6, (— — —) 7, (• • •) 8.

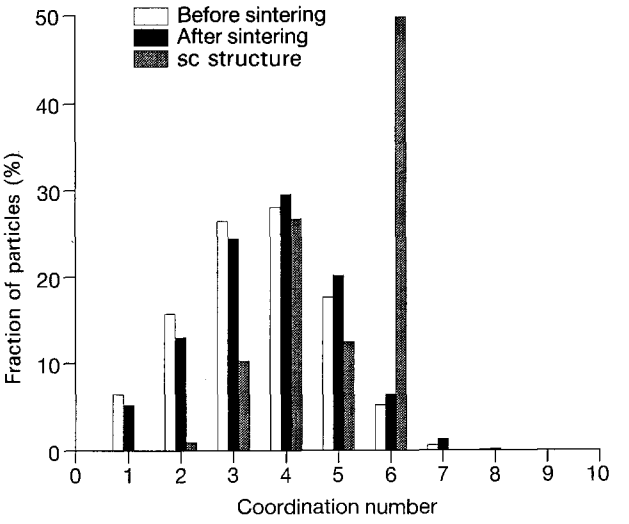

Figure 5 Distribution of coordination numbers in the random packing before and after sintering compared with that for the s c structure (1).

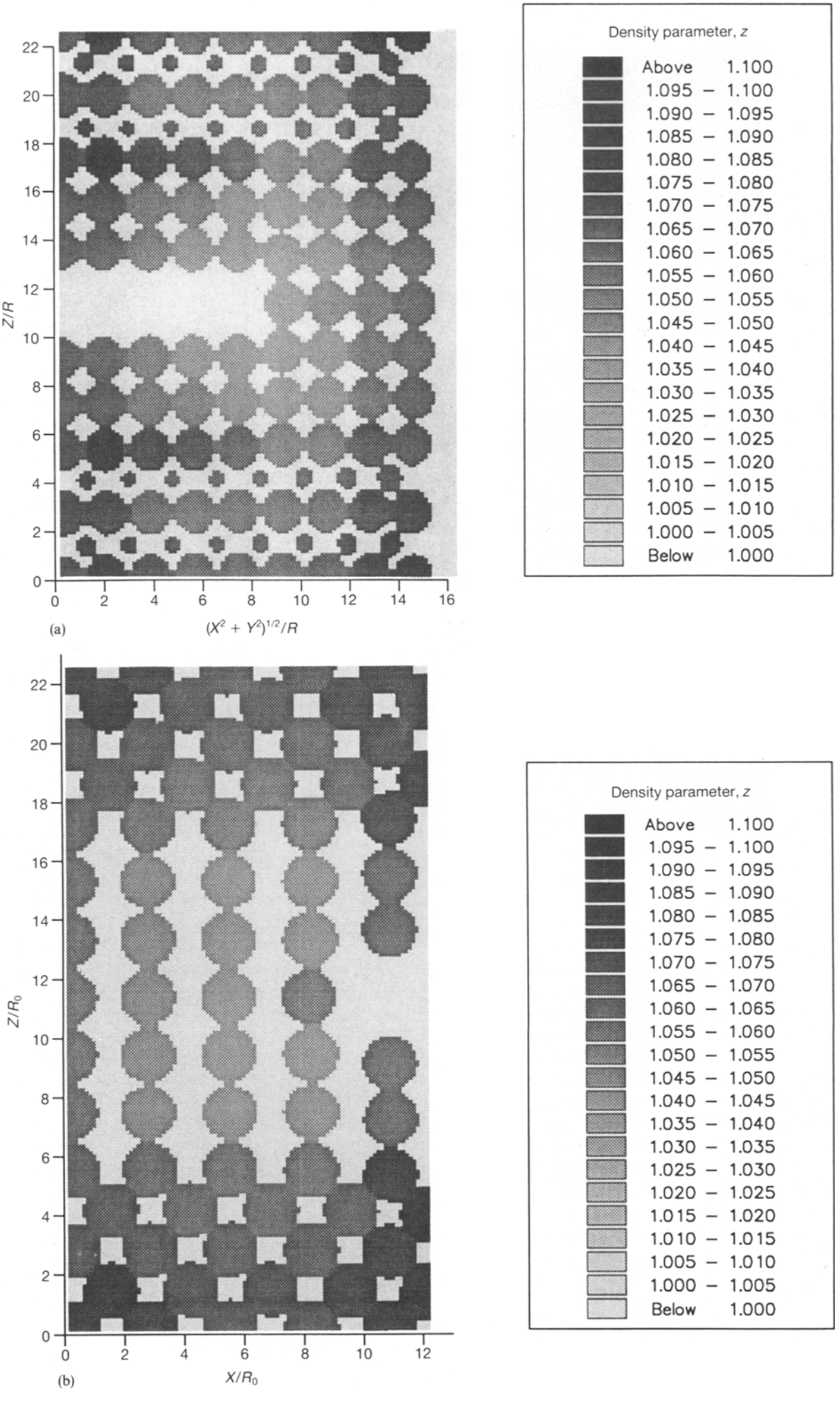

Figure 6 Local density prameter, z. (a) The vertical diagonal plane of structure 5, (b) the middle XZ plane of structure 6, and (c) the middle YZ plane of structure 7.

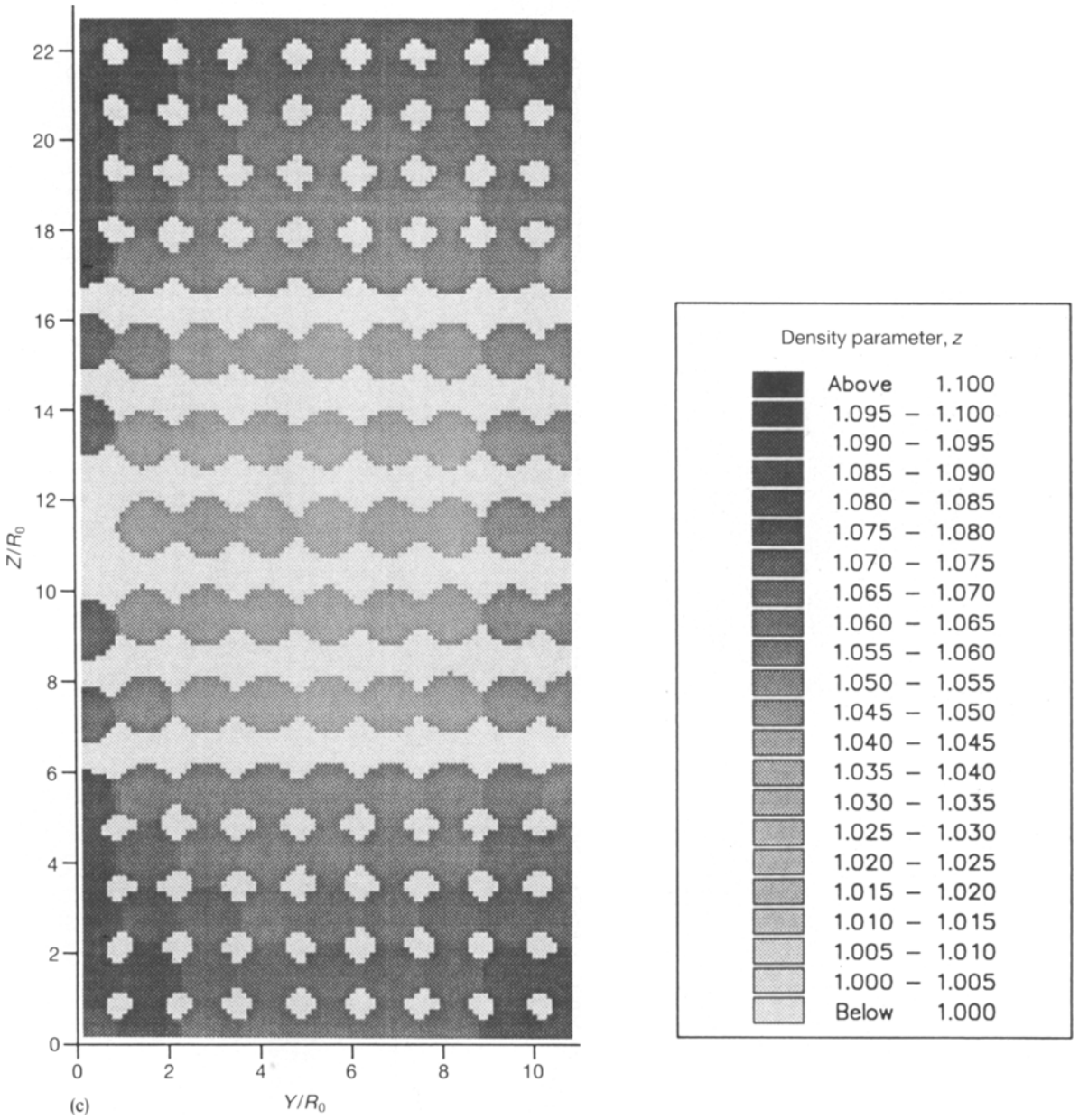

Figure 6 (continued)

packing, according to their coordination number is shown. In order to allow a comparison with the s c structure (1), we also plotted the data beginning to this structure. The majority of the particles in the s c structure, of course, has a coordidnation number of 6; particles with lower coordination can be found at the surface of the packing. The random packing shows a significant amount of particles with one or two nearest neighbours. Further, it can be observed that, even after sintering, no particles with coordination number higher than 8 are present. Again, this indicates that this packing consists of many small clusters.

Finally, some features of the sintered structures will be discussed qualitatively. In Fig. 6a, the density parameter, z_i, in the vertical diagonal ($X = Y$) plane of structure 5 is shown. This plot has been obtained by imposing a 100×200 grid on this plane. Each grid point has been assigned the z value of the nearest particle if it is overlapped by one or more particles and receives the value 0 if it is not covered by any particle. Before sintering, the particles in the second and the fourth (f c c) layer from the bottom and from the top did not cut the depicted plane but in the sintered structure the particles have moved through this plane and what we actually see in the second and the fourth layer of the stacking are the cross-sections of the necks of these particles. The row of vacancies is situated in the depicted plane and thus appears as a gap. It can be observed that, during the sintering, this gap has widened and this widening is most enhanced at the surface of the packing. The local density, as could be expected, increases going from the centre to the surface of the packing but in the third plane from the bottom and in the third plane from the top, some particles with an extraordinary density can be observed. These provide a nice example of the effects that local defects (in this case: a row of five vacancies) can have on the sintering behaviour of the bulk material in the near vicinity of the defects. Fig. 6b represents the middle XZ plane of structure 6 after sintering. The small gap at the right side of the structure is due to a vacancy in the middle of a row of nine, perpendicular

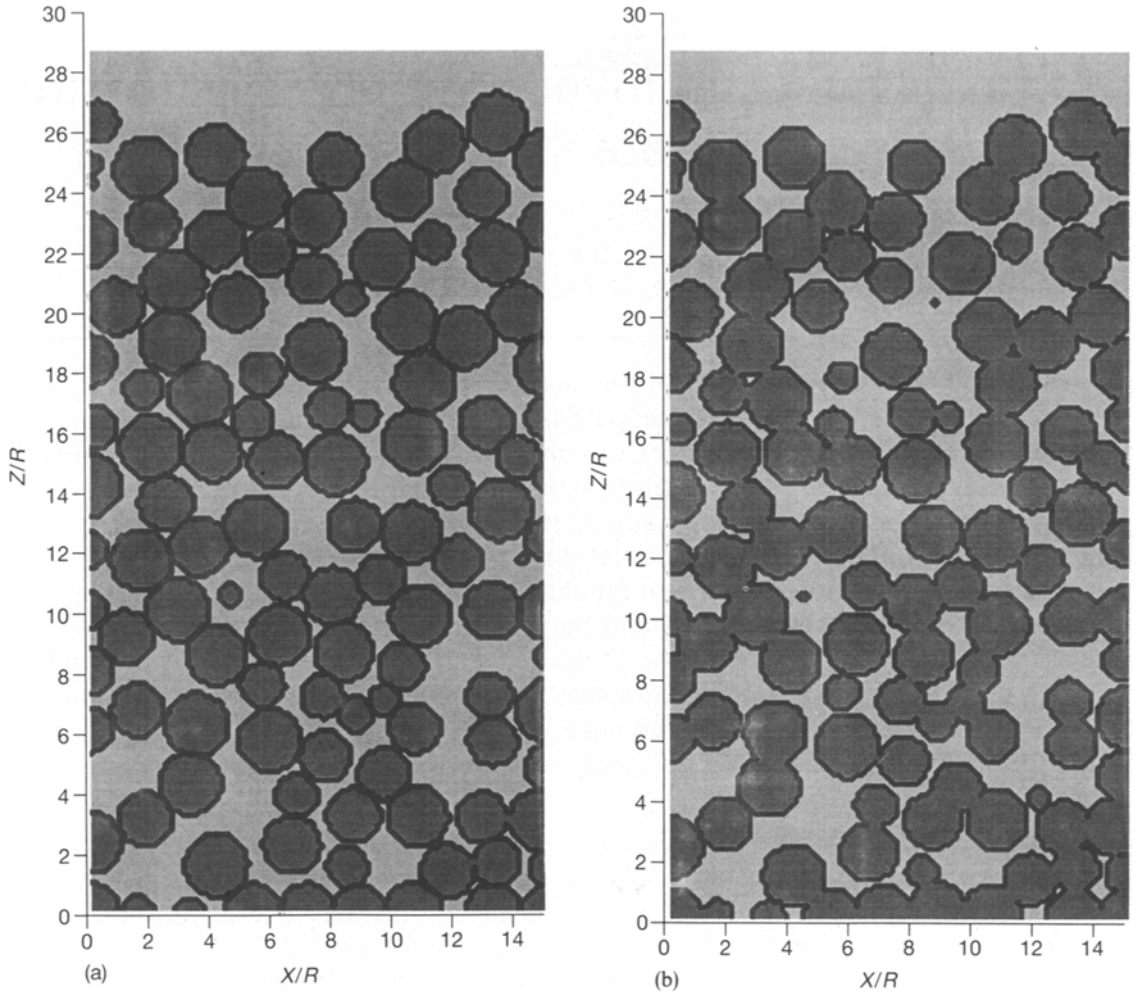

Figure 7 Cross-section of the random packing 8, (a) before sintering, (b) after sintering.

to the plane of the paper and its width has increased due to the sintering. Again, next to an overall contraction controlled by the external surface of the packing, local inhomogeneities in the density caused by the vacancy defects can be observed. Fig. 6c shows the density parameter z in the middle YZ plane of structure 7 after sintering. In this plane, the parts with the f c c structure appear rather massive because the plane cuts two rows of particles in each layer. Again, a widening of the gap and density fluctuations in the region surrounding the gap, can be observed. Finally in Fig. 7, we show a vertical slice of the random packing, before and after sintering. The two pictures provide some examples of the sintering-induced formation of isolated particles and isolated clusters of particles, as mentioned above.

5. Conclusions

A new simulation model for sintering in three-dimensional powder compacts is presented. Based on two-sphere sintering interactions, the model represents a multi-particle approach of structural reorganization effects, occurring during sintering, in packings of spherical particles. The simulations of the powder compacts used in this work (based on crystalline structures) show that the model adequately describes the reorganization effects that may result from local defects that are present before sintering.

References

1. J. FRENKEL, *J. Phys. (USSR)* **9** (1945) 385.
2. G. PETZOW and H. E. EXNER, *Z. Metallkde* **67** (1976) 611.
3. M. W. WEISER and L. C. DE JONGHE, *J. Am. Ceram. Soc.* **69** (1986) 822.
4. E. G. LINIGER and R. RAY, *Commun. Am. Ceram. Soc.* **79** (1988) C-408.
5. *Idem, Sci. Sintering* **21** (1989) 109.
6. E. ARZT, *Acta Metall.* **30** (1982) 1883.
7. J. W. ROSS, W. A. MILLER and G. C. WEATHERLY, *ibid.* **30** (1982) 203.
8. H. J. LEU, T. HARE and R. O. SCATTERGOOD, *ibid.* **36** (1988) 1977.
9. R. L. COBLE, *J. Appl. Phys.* **32** (1961) 787.
10. W. D. KINGERY and M. BERG, *ibid.* **26** (1955) 1205.
11. H. E. EXNER, *Rev. Powder Metall. Phys. Ceram.* **1** (1979) 1.
12. S. E. KOONIN and D. C. MEREDITH, in "Computational Physics" (Addison-Wesley New York, 1990) p. 29.
13. H. J. VERINGA, *J. Mater. Sci.* **26** (1991) 5985.
14. W. SOPPE, *Powder Technol.* **62** (1990) 189.

Received 17 November 1992
and accepted 8 July 1993